IET Renewable Power Generation

Research Article

IET Journals
The Institution of Engineering and Technology

Coordinated control of parallel operated renewable-energy-based DG systems

ISSN 1752-1416
Received on 25th January 2018
Revised 17th May 2018
Accepted on 06th July 2018
E-First on 31st August 2018
doi: 10.1049/iet-rpg.2018.5287
www.ietdl.org

Rajasekhararedy Chilipi[1], Naji Alsayari[1] ✉, Abdelali El Aroudi[2]

[1]Electrical Engineering Department, The Petroleum Institute Campus, Khalifa University of Science and Technology, Abu Dhabi, United Arab Emirates

[2]Departament d'Enginyeria Electrònica, Universitat Rovira i Virgili, Tarragona, Spain

✉ *E-mail: naji.alsayari@ku.ac.ae*

Abstract: This study proposes a coordinated control algorithm for two parallel-operated distributed generation (DG) systems fed from different renewable energy sources. The control algorithm ensures accurate control of reference active power generation from the inverters in the DG systems. In addition to reference power generation, the control algorithm also offers compensation of harmonics and reactive currents of the local loads by utilising the remaining capacities of the inverters in the DG systems. For this purpose, the control algorithm estimates compensating factors for each inverter based on the distributed harmonic and reactive currents. The inverter with a higher surplus capacity contributes to higher compensation and vice versa. The harmonic and reactive currents of the load are extracted using least mean mixed-norm adaptive algorithm for effective compensation. Furthermore, the control algorithm automatically switches to low-voltage ride through (LVRT) on sensing the grid faults. During LVRT, the active power generation by the inverters in DG systems is reduced and reactive currents are injected to support the grid recovery. The proposed control scheme is thoroughly investigated using computer simulations and hardware-in-the-loop-based experiments to show its feasibility and effectiveness.

1 Introduction

Owing to their eco-friendly nature, distributed generation (DG) systems based on renewable energy sources (RESs) such as wind turbines, solar photo-voltaic (PV) panels and fuel cells are being considered as a great alternative to fill the gap between the increasingly growing energy demand and the supply [1–3]. These DG systems are usually connected to the utility network and can also feed the local loads [4]. The power electronic interfaces [5] and their control system [6] are vital for DG systems to successfully harness the energy from RESs. It is well known that in order to interface the DG systems to the utility grid, voltage-source inverters (VSIs) are widely employed [7]. The primary objective of these inverters in DG systems is to feed the power extracted from RESs to either the loads in the case of an isolated system [8] or the grid in the case of grid-tied systems [9].

With the advent and widespread use of power electronic switches, the majority of the domestic loads that is drawing power from the distribution utility network are non-linear in nature. The harmonic currents generated by the non-linear loads can cause adverse effects such as voltage distortion and the excessive power losses. The effect of harmonic currents is much severe in case of low-voltage networks with high line impedance as the percentage of harmonic drop caused is larger. The effects of harmonics can be alleviated by installing active power filters (APFs) near non-linear loads. Instead of installing dedicated APFs to improve the power quality, the inverters of the DG units can be programmed to carry out harmonic currents compensation. The main advantage of using the inverters of DGs for active harmonic mitigation and reactive power compensation is that the network operator can avoid the use of dedicated static compensators such as APFs for this function, and therefore the solution is cost effective. The financial benefits of utilising the DG units for power quality improvement are discussed in [10].

In addition to real power generation, the DG systems can be integrated with secondary functions such as harmonic currents compensation [11, 12], reactive power compensation and voltage support [13] to improve power quality at the point of common coupling (PCC). Such DG systems are referred to as multifunctional DG (MFDG) systems [14]. Over the last two decades, several MFDG systems have been investigated. In [15], multifunctional grid-connected multilevel inverter topologies under different control strategies have been studied. In [16], predictive current control of multifunctional grid-connected solar energy fed inverter is discussed. A comparative study of various current detection algorithms for PV-based multifunctional APF has been conducted in [17]. On compensating the harmonic and reactive currents drawn by the local loads, the voltage and power factor at the PCC get improved. In [18], fuzzy-logic-based predictive direct power control of a grid-connected PV-based DG system with active power filtering capability has been reported.

To incorporate the aforementioned secondary functions in the inverter of a DG system, its control system must be provided with the information of harmonic and reactive components of the loads. A wide variety of methods for extracting the harmonic components from the load current can be found in the literature [19]. These can be broadly classified as time-domain and frequency-domain methods. Compared to frequency-domain methods, the time-domain ones are easy to implement. In time domain, synchronously rotating d–q frame (SRF) theory and instantaneous reactive power theory (IRPT) are quite popular methods. Wind-energy-based MFDG systems employing d–q frame theory and instantaneous p–q-theory-based extraction techniques for harmonic filtering are reported in [20, 21], respectively. The harmonics extraction methods employing pre-filters such as adaptive noise cancellation filters [22], sinusoidal signal integrators (SSIs) [23], adaptive notch filters [24] and least mean squares (LMSs) [25] also come under time-domain methods. Unlike, SRF and IRPT methods, pre-filters-based methods can be easily applied to single-phase systems. The LMS method has an added advantage compared with SSI-based pre-filters as they provide root mean square (RMS) values of the harmonics extracted which is extremely useful when the selective and dominant harmonic compensation is required. In addition to harmonic and reactive currents compensation, it is also expected that the inverters in grid-tied DG systems must possess low-voltage ride through (LVRT) capability to aid the grid recovery during faults. In the event of grid faults, the inverter in the DG system reduces the active power generation and starts injecting the reactive

power as defined by the grid codes [26]. In [27], fault ride through capability for grid-interfacing large-scale PV power plants has been discussed. In [28], a wavelet-fuzzy-neural-network-based active and reactive powers control for a grid-tied PV system during grid faults has been proposed. In [29], sliding-mode control-based LVRT of doubly fed induction generator (DFIG) system was implemented.

Owing to the sporadic nature of RESs, the inverters in DG systems seldom operate at their full capacity. Therefore, it is possible that the inverters could offer more compensation when they are lightly loaded, and vice versa. The idea of utilising only the remaining capacity of the inverter in a DG system for compensating purposes has been reported in [22, 30], where it has been demonstrated that the inverter can even offer partial/variable compensation when the remaining capacity is not sufficient. So far, the concept of contributing the remaining capacity of the inverter of a DG system for compensating purposes has only been applied to a single DG system. The concept of utilising the remaining capacity is promising and viable only with multiple DG systems, because if one of them reduces its compensation action due to peak power generation, other DGs with less power generation could take up the compensation action. With the probability that all DG units being fully loaded being very low, one can expect the continuity in compensation services. Consequently, this paper is a step forward for the development and implementation of a coordinated control algorithm that takes the scenario of two or more parallel DG systems into account. In coordinated control of multiple DG units, one has to consider various implementation issues such as communication, management and supervision. The control systems without interunit communication are preferred as they increase the system reliability.

Various studies dealing with the coordinated control of the multiple DG inverters can be found in literatures [31–34]. A control architecture to coordinate the DG systems and APFs of an isolated micro-grid is reported in [31]. APFs are installed to support the DGs in harmonic compensation and avoid the overloading of interface inverters and their performances are demonstrated only through simulation studies. In [32], coordinated control of multifunctional grid-tied inverters without interunit communication is proposed. This method fixes the compensation capacity that can be offered by the DG units regardless of loading condition and does not consider the intermittent nature of the RESs. In such cases, the inverters must be rated more than its peak fundamental power generation capacity. When the compensating capacity is fixed, it limits the full utilisation of remaining capacity even when the inverter is lightly loaded. A centralised control for MFDG units is implemented in [33], where the inverters of DG systems are used to compensate certain dedicated loads. No method for spontaneous sharing of harmonic and reactive current is proposed and to provide compensation for the loads other than dedicated, interunit communication required. Another work on coordinated control of multiple multifunctional grid-connected converters in micro-grid is reported in [34]. Here, sequential allocation of the DG inverters' remaining capacity for harmonic and reactive currents compensation is suggested. For instance, the inverter of second DG has to wait until the inverter of first DG is fully utilised and so on. Therefore, interunit communication is required for this method.

Considering the limitations of existing coordinated control methods such as interunit communication and restricting the studies to computer simulations, this paper adopts a simple and effective conductance (H)–volt-Ampere (VA) rating (S) droop-based method for dynamically sharing the harmonic and reactive currents. The H–S droop-based control of multiple APFs is reported in [35], where the harmonic VA that needs to be compensated is shared among multiple APFs proportional to their kVA ratings. Similarly, the proposed control applies the H–S droop-based sharing of compensating currents proportional to the remaining capacities of the DG inverters. Thus, the shared harmonic and reactive currents will be compensated until the inverters' capacities are fully utilised without interunit communication. This control algorithm can also be easily extended to any number of systems. Unlike the works reported in [22, 30], the proposed control algorithm comes with an essential LVRT capability which will be enabled on sensing the reduction in PCC voltages and offers seamless transition between LVRT mode and normal mode of operation. An adaptive filtering method known as least mean mixed-norm (LMMN) algorithm is adopted and modified as per the requirements to extract the harmonic and reactive current components. This algorithm combines the advantages of LMS [30] and least mean fourth (LMF) techniques [36]. The LMS-based adaptive algorithm works on the principle of minimising the squared error. Hence, the LMS algorithm is more effective when the error is <1.0 and it becomes less responsive when the error is >1.0. The LMF algorithm is based on minimising the fourth power of the error and it is more effective when the error is >1.0 compared with the LMS algorithm. Similar to the LMS technique, the LMMN algorithm also gives instantaneous and RMS values of the harmonics during decomposition process. Using the outputs of LMMN algorithm, the proposed coordinated control is realised to estimate the reference currents for the control of grid-interfacing inverters. The efficacy of the proposed control under various testing conditions is demonstrated using simulation and experimental results.

On the basis of the previous discussion, the main features of the present work are summarised as follows:

i. Coordinated control of VSIs in the DG units to share compensation efforts without affecting the real power export.
ii. Only the remaining capacity of the VSIs is considered for harmonic and reactive power compensation.
iii. A simple and effective droop-based method is proposed for dynamically sharing the harmonic and reactive currents.
iv. Estimation of harmonic and reactive current using LMMN identification algorithm.
v. Seamless transition between LVRT and normal modes of operation.

2 System description and principle of operation

The system configuration of parallel-operated DG systems connected to the utility grid is depicted in Fig. 1. The system consists of two single-phase inverters, namely VSI-1 and VSI-2 connected to the PCC through coupling inductors, and local linear/non-linear loads. The ac side currents of the DG1 inverter and DG2 inverter are represented as i_{DG1} and i_{DG2}, respectively. The voltage of the single-phase grid is denoted as v_g and the corresponding PCC voltage is labelled as v. The source/grid current is denoted as i_g and the current drawn by local loads is denoted as i_l. This load current i_l is typically composed of fundamental active (i_{l1p}), fundamental reactive (i_{l1q}) and harmonic components (i_{lh}) as $i_l = i_{l1p} + i_{l1q} + i_{lh}$. It is assumed that the input dc-link voltages of the DG inverters are maintained constant by DG sources. The sources of the DG1 inverter and DG2 inverter may be comprised of different RESs. Therefore, the active powers generated by the inverters may not be equal.

To inject the active power extracted from RES into the grid and simultaneously compensate the harmonic (i_{lh}) and reactive currents (i_{l1q}) drawn by the local loads, both inverters are operated in current mode control. In this mode, if the PCC voltage is assumed to be constant, the active power injected by the inverters is proportional to their active current components. The instantaneous currents on the ac sides of the DG1 inverter and DG2 inverter can be expressed as $i_{DG1} = i_{P1} + i_{com1}$ and $i_{DG2} = i_{P2} + i_{com2}$, respectively. The currents i_{P1} and i_{P2} account for the injected active powers. The currents i_{com1} and i_{com2} are the compensating currents offered by the inverters.

3 Control algorithm

The proposed control algorithm for coordinated control of inverters in parallel-connected DG systems is shown in Fig. 2. The control algorithm realises reference currents for the inverters in both DG systems simultaneously. The reference signals estimated by the control algorithm are composed of the following components:

i. Reference active power generation currents.
ii. Reference compensating currents.
iii. Reference LVRT currents.

The estimation of these currents is illustrated in the forthcoming sections.

3.1 Reference active power generation currents

The reference powers to the DG1 inverter and the DG2 inverter are represented as P^*_{DG1} and P^*_{DG2}, respectively. The reference powers are compared with the respective actual output powers of the DG1 inverter and the DG2 inverter and then the obtained power errors are processed through two different proportional plus integral (PI) controllers whose outputs represent the amplitudes of reference active power generation currents to be injected by the inverters in DG1 and DG2 as given as below:

$$I^*_{P1} = K_{p1}(P^*_{DG1} - P_{DG1}) + K_{i1}\int (P^*_{DG1} - P_{DG1})\,dt \tag{1a}$$

$$I^*_{P2} = K_{p2}(P^*_{DG2} - P_{DG2}) + K_{i2}\int (P^*_{DG2} - P_{DG2})\,dt \tag{1b}$$

where K_{p1}, K_{p2} and K_{i1}, K_{i2} are the proportional and integral gain constants of the PI controllers, respectively.

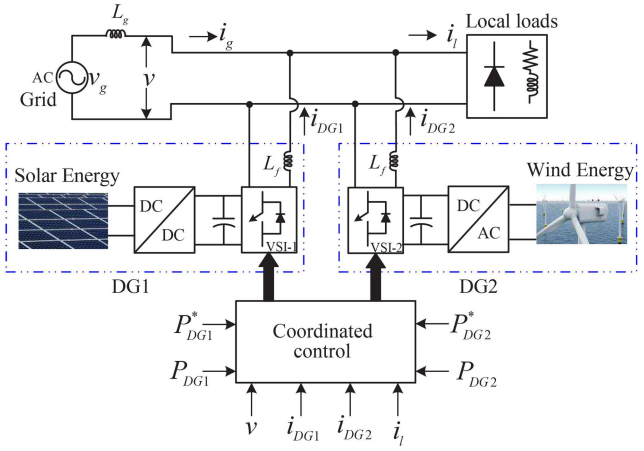

Fig. 1 *Schematic diagram of two grid-connected inverters supplied by two different RESs under coordinated control*

The outputs of the PI controllers given in (1) are multiplied with the in-phase unit template of fundamental PCC voltage ($\sin\omega_1 t$) to estimate the instantaneous reference active power generation currents of the DG1 inverter and the DG2 inverter

$$i^*_{P1} = I^*_{P1} \times \sin\omega_1 t\,. \tag{2a}$$

$$i^*_{P2} = I^*_{P2} \times \sin\omega_1 t\,. \tag{2b}$$

The in-phase unit template $\sin\omega_1 t$ is obtained by employing a single-phase phase-locked loop [22] over the PCC voltage.

3.2 Reference compensating currents

As stated before, the load current i_l can be decomposed into various components such as fundamental active (i_{l1p}), fundamental reactive (i_{l1q}) and harmonic (i_{lh}) components. To ensure power quality at PCC, the grid should be free from i_{l1q} and i_{lh}. Therefore, the inverters of the DG systems inject compensating currents to cancel the currents i_{l1q} and i_{lh} drawn by local loads. Since the inverters of DG systems inject compensating currents based on their remaining capacities, the reference compensating currents of the DG1 inverter and the DG2 inverter are estimated as follows:

$$i^*_{com1} = G_{q1} \times i_{l1q} + G_{h1} \times i_{lh} \tag{3a}$$

$$i^*_{com2} = G_{q2} \times i_{l1q} + G_{h2} \times i_{lh} \tag{3b}$$

where G_{h1}, G_{h2} and G_{q1}, G_{q2} are the harmonic and reactive current compensating factors, respectively, of the DG1 inverter and the DG2 inverter and they indicate the amount of compensation being offered by the inverters. For example, if G_{h1}, G_{h2} are found to be 0.6 and 0.4, respectively, the DG1 inverter and the DG2 inverter are compensating 60 and 40% of i_{lh}, respectively. The values of compensating factors depend on the active power generation of the inverters and the RMS values of i_{l1q} and i_{lh}. Therefore, it is required to estimate/extract the currents i_{l1q} and i_{lh} and their RMS values I_{l1q} and I_{lh} for compensating purposes. To achieve this, an LMMN-based system identification adaptive algorithm has been employed in the present paper.

3.2.1 LMMN algorithm: Fig. 3 shows the decomposition process of load current i_l into active (i_{l1p}), reactive (i_{l1q}) and harmonic (i_{lh}) components using LMMN-based adaptive algorithm. The principle of LMMN algorithm is based on the minimisation of a cost

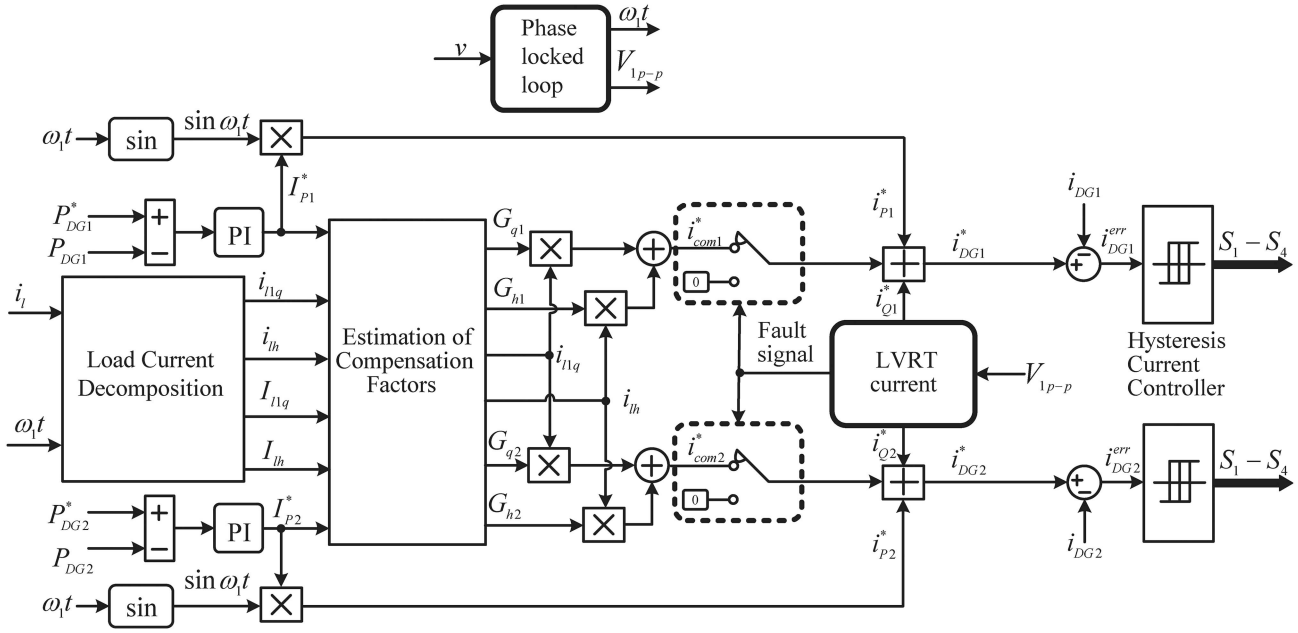

Fig. 2 *Detailed block diagram of the coordinated control of DG systems*

function defined as the convex combination of the squared and fourth powers of the error norms [36]

$$J(k) = \lambda E\{e(k)^2\} + (1-\lambda)E\{e(k)^4\} \quad (4)$$

where $e(k)$ is the output error, $E\{.\}$ stands for the mathematical expectation, $\lambda\epsilon[0 \quad 1]$ is the mixing parameter and k is the sample index in discrete time. When $\lambda = 1$, expression (4) becomes the error norm for the LMS algorithm, whereas for $\lambda = 0$, (4) transforms into the error norm for the LMF algorithm. Judicious choice of λ offers the algorithm an intermediate performance between that of LMS and LMF. Thus, one can fully utilise advantages of both the LMS and the LMF algorithms in LMMN algorithm by properly selecting the parameter λ. The output error of LMMN-based identification algorithm is defined as follows:

$$e(k) = d(k) - \boldsymbol{W}^{\mathrm{T}}(k)\boldsymbol{X}(k) \quad (5)$$

where $\boldsymbol{X}(k)$ denotes the input vector, $\boldsymbol{W}(k)$ is the vector of adaptive weights of $d(k)$ represents the desired response.

The weight update expression for the LMMN algorithm is derived from the following steepest descent type weight update equation:

$$\boldsymbol{W}(k+1) = \boldsymbol{W}(k) - \mu(\nabla_{W(k)})J(k) \quad (6)$$

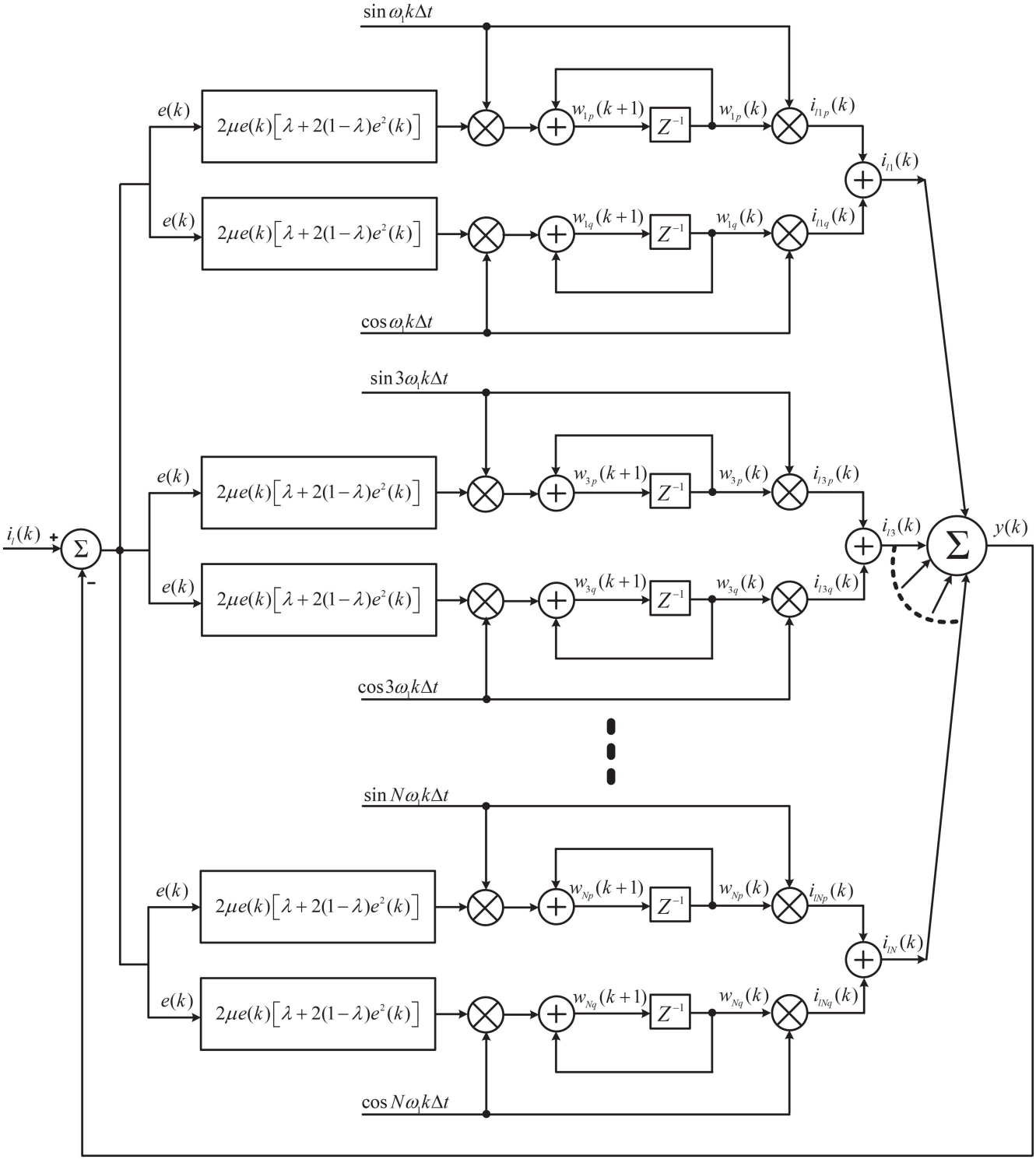

Fig. 3 *Load current decomposition using LMMN algorithm*

where μ is the learning rate and $\nabla_{W(k)}J(k)$ is the instantaneous gradient of $J(k)$ which is evaluated at the present value of $\boldsymbol{W}(k)$.

Differentiating (6) with respect to $\boldsymbol{W}(k)$ would yield the weight updating expression of LMMN algorithm

$$\boldsymbol{W}(k+1) = \boldsymbol{W}(k) + 2\mu e(k)\big(\lambda + 2(1-\lambda)e^2(k)\big)\boldsymbol{X}(k) \tag{7}$$

When the LMMN algorithm is adopted for extracting various harmonic components from the load current as shown in Fig. 3, the load current $i_{\rm l}(k)$ represents the desired signal $d(k)$ and then the input vector $\boldsymbol{X}(k)$ and the weight vector $\boldsymbol{W}(k)$ are defined as follows:

$$\begin{aligned}\boldsymbol{X}(k) &= \begin{bmatrix}\boldsymbol{x}_1(k) & \boldsymbol{x}_2(k) & \boldsymbol{x}_3(k) & \dots & \boldsymbol{x}_N(k)\end{bmatrix}^{\rm T}\\ \boldsymbol{x}_1(k) &= \begin{bmatrix}\sin\omega_{\rm l}k\Delta t & \cos\omega_{\rm l}k\Delta t\end{bmatrix}^{\rm T}\end{aligned} \tag{8}$$

$$\begin{aligned}\boldsymbol{W}(k) &= \begin{bmatrix}\boldsymbol{w}_1(k) & \boldsymbol{w}_2(k) & \boldsymbol{w}_3(k) & \dots & \boldsymbol{w}_N(k)\end{bmatrix}^{\rm T}\\ \boldsymbol{w}_1(k) &= \begin{bmatrix}w_{1p}(k) & w_{1q}(k)\end{bmatrix}^{\rm T}\end{aligned} \tag{9}$$

Using (8) and (9), the output error and weights updating expressions given by (5) and (7) can be rewritten as follows:

$$\begin{aligned}e(k) = {} & i_{\rm l}(k)\\ & -\begin{bmatrix}w_{1\rm p}(k) & w_{1q}(k) & w_{3\rm p}(k) & w_{3q}(k) & \dots & w_{N\rm p}(k) & w_{Nq}(k)\end{bmatrix}\\ & \times\begin{bmatrix}\sin\omega_{\rm l}k\Delta t\\ \cos\omega_{\rm l}k\Delta t\\ \sin 3\omega_{\rm l}k\Delta t\\ \cos 3\omega_{\rm l}k\Delta t\\ \dots\\ \sin N\omega_{\rm l}k\Delta t\\ \cos N\omega_{\rm l}k\Delta t\end{bmatrix}\end{aligned} \tag{10}$$

(see (11)) . From (10), various harmonic components of i_l extracted by the LMMN algorithm including fundamental component (i_{l1}) are expressed as

$$\begin{aligned}\begin{bmatrix}i_{\rm l1}(k)\\ i_{\rm l3}(k)\\ i_{\rm l5}(k)\\ \dots\\ i_{\rm lN}(k)\end{bmatrix} &= \begin{bmatrix}i_{\rm l1p}(k)+i_{\rm l1q}(k)\\ i_{\rm l3p}(k)+i_{\rm l3q}(k)\\ i_{\rm l5p}(k)+i_{\rm l5q}(k)\\ \dots\\ i_{\rm lNp}(k)+i_{\rm lNq}(k)\end{bmatrix}\\ &= \begin{bmatrix}w_{1\rm p}(k)\times\sin\omega_{\rm l}k\Delta t + w_{1q}(k)\times\cos\omega_{\rm l}k\Delta t\\ w_{3\rm p}(k)\times\sin 3\omega_{\rm l}k\Delta t + w_{3q}(k)\times\cos 3\omega_{\rm l}k\Delta t\\ w_{5\rm p}(k)\times\sin 5\omega_{\rm l}k\Delta t + w_{5q}(k)\times\cos 5\omega_{\rm l}k\Delta t\\ \dots\\ w_{N\rm p}(k)\times\sin N\omega_{\rm l}k\Delta t + w_{Nq}(k)\times\cos N\omega_{\rm l}k\Delta t\end{bmatrix}\end{aligned} \tag{12}$$

A careful observation of (12) reveals that the weight vector $\boldsymbol{W}(k)$ indeed represents the Fourier coefficients of the load current components. Therefore, using the weights given in (11), the RMS values of the reactive component and various harmonics components can be deduced and are expressed as follows:

$$\begin{bmatrix}I_{\rm l1q}\\ I_{\rm l3}\\ I_{\rm l5}\\ \dots\\ I_{\rm lN}\end{bmatrix} = \begin{bmatrix}w_{1q}/\sqrt{2}\\ \sqrt{(w_{3\rm p})^2+(w_{3q})^2}/\sqrt{2}\\ \sqrt{(w_{5\rm p})^2+(w_{5q})^2}/\sqrt{2}\\ \dots\\ \sqrt{(w_{N\rm p})^2+(w_{Nq})^2}/\sqrt{2}\end{bmatrix}. \tag{13}$$

Using (13), the RMS value of $i_{\rm lh}$ in the load current can be estimated as

$$I_{\rm lh} = \sqrt{(I_{\rm l3})^2+(I_{\rm l5})^2+\dots+(I_{\rm lN})^2} \tag{14}$$

It should be noted that the present paper has considered odd harmonics only. However, a similar procedure can be followed to extract even harmonics when required.

3.2.2 Estimation of compensation factors: Before proceeding to the estimation of the compensation factors, first the extracted reactive and harmonic components must be distributed between the DG1 inverter and the DG2 inverter and this is accomplished using the droop characteristic, between the harmonic conductance (H) and the VA capacity (S). In [35], the H–S droop-based sharing is adopted for the control of multiple APFs which is now being employed for achieving even distribution of compensation efforts among the multiple DG units.

$$\begin{aligned}\underbrace{\begin{bmatrix}w_{1\rm p}(k+1)\\ w_{1q}(k+1)\\ w_{3\rm p}(k+1)\\ w_{3q}(k+1)\\ \dots\\ w_{N\rm p}(k+1)\\ w_{Nq}(k+1)\end{bmatrix}}_{\boldsymbol{W}(k+1)} &= \underbrace{\begin{bmatrix}w_{1\rm p}(k)\\ w_{1q}(k)\\ w_{3\rm p}(k)\\ w_{3q}(k)\\ \dots\\ w_{N\rm p}(k)\\ w_{Nq}(k)\end{bmatrix}}_{\boldsymbol{W}(k)}\\ &+2\mu e(k)\times\big\{\lambda+2(1-\lambda)e^2(k)\big\}\\ &\times\underbrace{\begin{bmatrix}\sin\omega_{\rm l}k\Delta t\\ \cos\omega_{\rm l}k\Delta t\\ \sin 3\omega_{\rm l}k\Delta t\\ \cos 3\omega_{\rm l}k\Delta t\\ \dots\\ \sin N\omega_{\rm l}k\Delta t\\ \cos N\omega_{\rm l}k\Delta t\end{bmatrix}}_{\boldsymbol{X}(k)}\end{aligned} \tag{11}$$

The *H–S* droop characteristics of both DG units can be defined as follows:

$$b_1 \times S'_{r1} = b_2 \times S'_{r2} \tag{15}$$

where S'_{r1} and S'_{r2} are the remaining capacities of the inverters of DG1 and DG2, respectively, and b_1 and b_2 are the droop coefficients.

The *H–S* droop control that is defined in (15) allows even sharing of harmonic/reactive VA between DG1 and DG2 as follows:

$$\frac{k_1}{S'_{r1}} = \frac{k_2}{S'_{r2}} \tag{16}$$

where k_1 and k_2 are the sharing factors of the DG1 inverter and the DG2 inverter, respectively, and they are given by

$$k_1 = \frac{S'_{r1}}{S'_{r1} + S'_{r2}}, \quad k_2 = \frac{S'_{r2}}{S'_{r1} + S'_{r2}}. \tag{17}$$

Since the dc-link voltages of the inverters in DG systems are assumed to be constant, their loading is decided by the current on their ac sides. The current should never exceed its rated value. One has to consider the remaining current capacities instead of S'_{r1} and S'_{r2}. If I_{r1} and I_{r2} are the rated currents of the DG1 inverter and the DG2 inverter, respectively, on allocating them for active power generation, the remaining current capacities are estimated as

$$I'_{r1} = \sqrt{I_{r1}^2 - (I^*_{P1}/\sqrt{2})^2}, \quad I'_{r2} = \sqrt{I_{r2}^2 - (I^*_{P2}/\sqrt{2})^2} \tag{18}$$

Using (18), expressions (16) and (17) are rewritten as

$$\frac{k_1}{I'_{r1}} = \frac{k_2}{I'_{r2}} \tag{19}$$

and

$$k_1 = \frac{I'_{r1}}{I'_{r1} + I'_{r2}}, \quad k_2 = \frac{I'_{r2}}{I'_{r1} + I'_{r2}}. \tag{20}$$

Once the sharing factors are calculated, the estimated harmonic and reactive currents are distributed between the inverters of DG1 and DG2 as follows:

$$x_{h1} = k_1 \times i_{lh}, \quad x_{q1} = k_1 \times i_{l1q} \tag{21}$$

$$x_{h2} = k_2 \times i_{lh}, \quad x_{q2} = k_2 \times i_{l1q} \tag{22}$$

where x_{h1}, x_{h2} and x_{q1}, x_{q2}, are the shared harmonic and reactive currents, respectively.

This way, the inverters in both DG systems will contribute to compensation as long as their remaining capacities are not equal to zero. However, a mere distribution of harmonic and reactive currents as given in (21) and (22) does not always guarantee full compensation because, even after distribution, the remaining capacities may not be sufficient to compensate the distributed harmonic and reactive currents. Therefore, it is required to estimate the compensating factors to know the amount of compensation that can be offered by the DG1 inverter and the DG2 inverter.

Let X_{h1} and X_{q1} be the RMS values of x_{h1} and x_{q1}, respectively, then the compensating factors for the DG1 inverter are estimated considering the following possible scenarios:

i. If $I'_{r1} = 0$, then the DG1 inverter has no remaining capacity to offer compensation and hence $G_{h1} = 0$ and $G_{q1} = 0$.
ii. If $I'_{r1} > 0$ and $I'_{r1} < X_{h1}$, then the DG1 inverter can only offer partial compensation of x_{h1} and zero compensation for x_{q1}, therefore, $G_{h1} = k_1 \times (I'_{r1}/X_{h1})$ and $G_{q1} = 0$.
iii. If $I'_{r1} > X_{h1}$ and $I'_{r1} < \sqrt{(X_{h1})^2 + (X_{q1})^2}$, then the DG1 inverter can fully compensate x_{h1} and offers partial compensation for x_{q1}, in this case $G_{h1} = k_1$ and $G_{q1} = k_1 \times \sqrt{\left((I'_{r1})^2 - (X_{h1})^2\right)/(X_{q1})^2}$.
iv. If $I'_{r1} \geq \sqrt{(X_{h1})^2 + (X_{q1})^2}$, then the DG1 inverter can fully compensate x_{h1} and x_{q1}, consequently, $G_{h1} = k_1$ and $G_{q1} = k_1$.

Similarly, the compensating factors G_{h2} and G_{q2} for DG2 inverter are calculated using I'_{r2}, X_{h2} and X_{q2}. Thus, the estimated factors are substituted in (3a) and (3b) to calculate the reference compensating currents of the DG1 inverter and the DG2 inverter, respectively.

The factors G_{h1}, G_{h2}, G_{q1} and G_{q2} can vary from 0 to 1 based on the level of compensation. To utilise the remaining capacities of the inverters, the harmonic currents are given first priority and will be compensated first. Once the harmonics are fully compensated, the control algorithm allows the inverters to compensate reactive current. Therefore, as long as the sum of factors G_{h1} and G_{h2} is less than unity, the reactive current compensation factors will be found zero. Under full compensation of i_{lh}, the sum $G_{h1} + G_{h2}$ becomes unity. Similarly, as long as the inverters in both DGs are collectively able to provide full reactive power compensation, then $G_{q1} + G_{q2}$ becomes unity. If both inverters are having equal remaining capacities, the allocations of i_{lh} and i_{l1q} becomes equal between the DG1 inverter and the DG2 inverter which will lead to $G_{h1} = G_{h2}$ and $G_{q1} = G_{q2}$.

3.3 LVRT currents

During grid faults, the voltage at the PCC will be affected. Once, the PCC voltage falls below 0.9 pu, the LVRT feature of the control algorithm will be activated to inject the reactive current into the grid as per the grid codes. In this paper, the German grid codes are being followed [26]. During low-voltage condition, the control algorithm gives preference to reactive current injection. Therefore, it may reduce the active current component of the DG1 inverter and the DG2 inverter to accommodate the LVRT current. Furthermore, the control algorithm sets the reference compensating currents of the inverters to zero as shown in Fig. 2. As soon as the fault is cleared, the active power generation of the inverters would be restored to the reference value with a gradient of at least 20% of the rated power per second. The magnitude of reactive current (I^*_D) to be injected by the inverters is computed based on the PCC voltage magnitude and according to grid codes

$$I^*_Q = \begin{cases} 0, & \text{if } V_m \geq 0.9. \\ \frac{9}{4} \times (0.9 - V_m) \times \sqrt{2} I_r, & \text{if } 0.5 < V_m < 0.9. \\ 0.9 \times \sqrt{2} I_r, & \text{if } V_m \leq 0.5. \end{cases} \tag{23}$$

where V_m is the magnitude of PCC voltage in pu and I_r is the rated current of an inverter.

Using I^*_Q estimated in (23), the amount of active power component that can be injected by an inverter during LVRT must be limited to

$$I_{lim} = \sqrt{(\sqrt{2} I_r)^2 - I_Q^2}. \tag{24}$$

The current given in (24) can be either greater than or less than the output of power PI controller I^*_P. Therefore, one has to choose the smallest between I_{lim} and I^*_P for active power generation during the LVRT situation as explained below:

$$I^*_P(k) = \begin{cases} I^*_P(k), & \text{if } I_{lim}(k) \geq I^*_P(k). \\ I_{lim}(k), & \text{if } I_{lim}(k) < I^*_P(k). \end{cases} \tag{25}$$

The instantaneous LVRT currents to be injected by the DG1 inverter and the DG2 inverter in quadrature with the PCC voltage during grid faults are

$$i^*_{Q1} = -I^*_{Q1} \times \cos \omega_1 t \tag{26a}$$

$$i^*_{Q2} = -I^*_{Q2} \times \cos \omega_1 t \tag{26b}$$

where $\cos \omega_1 t$ is the quadrature phase template of the fundamental PCC voltage.

3.4 Reference currents estimation

Various components required for the estimation of the reference currents of the DG1 inverter and the DG2 inverter are derived in the previous sections and are given in (2), (3) and (26). Using, those components, the reference currents for the control of the DG1 inverter and the DG2 inverter are obtained as

$$i^*_{DG1} = i^*_{P1} + i^*_{com1} + i^*_{Q1} \tag{27a}$$

$$i^*_{DG2} = i^*_{P2} + i^*_{com2} + i^*_{Q2} \tag{27b}$$

The reference currents (i^*_{DG1}, i^*_{DG2}) obtained in (27a) and (27b) are compared with their actual currents (i_{DG1}, i_{DG2}) to generate current errors. These current errors are processed with hysteresis blocks to develop switching patterns for both inverters in DG systems.

4 Results and performance evaluation

The performance of the proposed control algorithm for parallel-operated DG systems is discussed in this section via simulation and real-time hardware-in-the-loop (HIL)-based experimental results. The entire power system that is shown in Fig. 1 is developed in an HIL system. The proposed control algorithm is executed in a digital controller DS1202 at a sampling period of 30 μs. The parameters of the system that are used for both simulation and experimental studies are given in Table 1. It should be noted that for the sake of easy understanding and simplicity, same kVA rating is considered for both the inverters. Various possible testing scenarios have been considered to prove the efficacy of the control algorithm. The performance of the proposed control algorithm is initially demonstrated using simulation results and then corroborated with HIL-based experimental results.

Table 1 System and control parameters

Parameters	Values
rated PCC voltage	240 V
grid frequency	50 Hz
inverters' capacity	7.5 kVA
coupling inductance (L_f)	3.5 mH
dc-link voltage of the DG inverters	$V_{dc} = 400$ V
power PI controllers' gains	$K_{p1} = K_{p2} = 1.3 \times 10^{-3}$, $K_{i1} = K_{i2} = 0.28$.
loads	1−ϕ two-pulse controlled rectifier with series connected $R_l = 20\,\Omega$ and L_l = 300 mH on dc side
LMMN parameters	$\mu = 2 \times 10^{-3}$ and $\lambda = 0.8$
highest harmonic number N	25

4.1 Performance under a step change in active power generation

The performance during a step change in active power generation of the DG1 inverter and the DG2 inverter is shown in Figs. 4 and 5, respectively. The active powers generated by the inverters vary as their reference powers vary. Initially, the inverters in both DG systems are delivering active power at their rated capacity, i.e., 7.5 kW. Consequently, the harmonic and the reactive currents drawn by the non-linear loads are not compensated. Hence, the grid current i_g is non-sinusoidal. The power generated by the inverter in DG1 is first reduced to 7.3 kW from 7.5 kW while the power of the DG2 inverter is kept at 7.5 kW. Before the power change, the DG1 inverter current i_{DG1} is seen to be sinusoidal as it is not offering any compensation. Once the DG1 inverter power generation falls below the rated capacity, the control algorithm assigns its remaining capacity to compensate for the harmonic currents of the local loads. Still, harmonic distortion in grid current can be seen here as the DG1 inverter could not offer full compensation of the load harmonics with its remaining capacity. Fig. 5 shows the system performance as the power generated by the DG2 inverter is reduced from 7.5 to 7.3 kW while DG1 inverter power is maintained at 7.3 kW. Now, the DG2 inverter also contributes to compensation, and hence the current i_g is seen to be sinusoidal. Furthermore, the current i_g is exactly out of phase with the PCC voltage v indicating the unity power factor operation.

The waveforms of PCC voltage, grid currents and their harmonic spectra are shown in Fig. 6 while DG1 and DG2 are generating real power at their rated capacity. Since the harmonic currents drawn by the non-linear loads are not being compensated, distortion in PCC voltage v and grid current i_g can be seen. The total harmonic distortions (THDs) of PCC voltage and grid current are found to be 6.13 and 23.85%, respectively. The waveforms and the harmonic spectra of v and i_g with $P_{DG1} = P_{DG2} = 7.3$ kW are shown in Fig. 7. Since the real power generation is reduced, the remaining capacities of the inverters are spent in providing compensation of harmonic and reactive currents. Hence, the waveforms of PCC voltage and grid currents are seen distortion free and their THDs are found to be 1.95 and 2.90% which are well below the recommended limits of IEEE-519 standards.

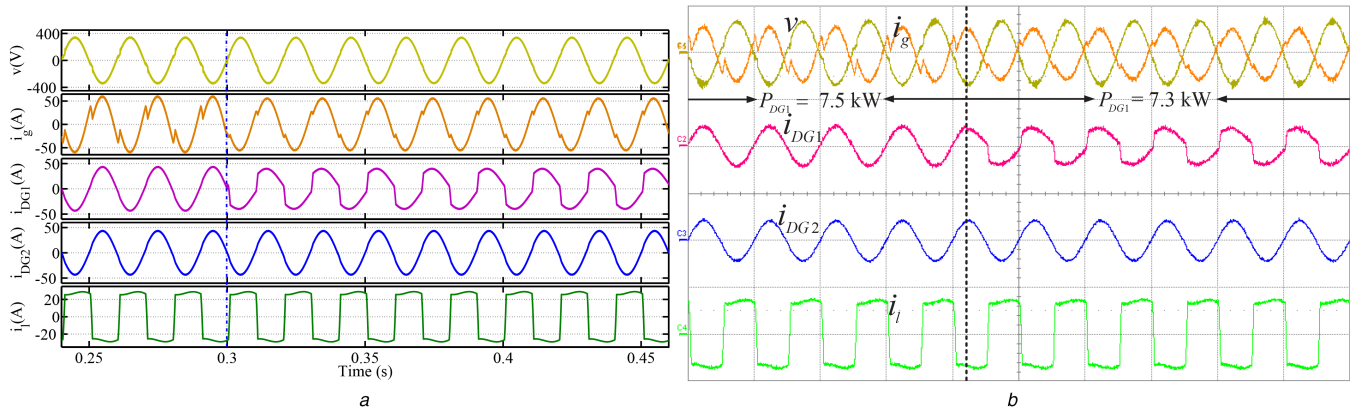

Fig. 4 *Performance under a step change in P_{DG1} from 7.5 to 7.3 kW with $P_{DG2} = 7.5$ kW*

(a) Simulation results, ***(b)*** Experimental results

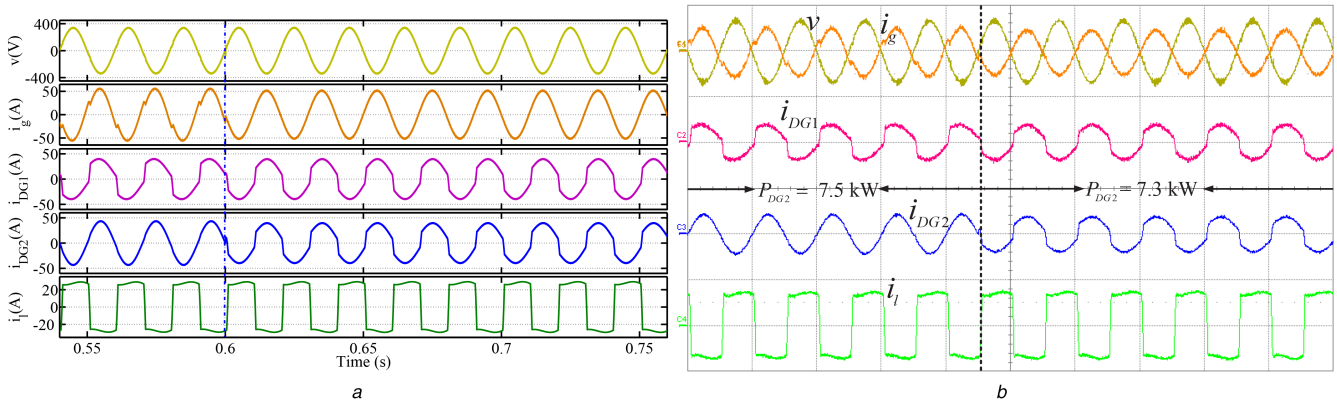

Fig. 5 *Performance under a step change in P_{DG2} from 7.5 to 7.3 kW with $P_{DG1} = 7.3$ kW*
(a) Simulation results, ***(b)*** Experimental results

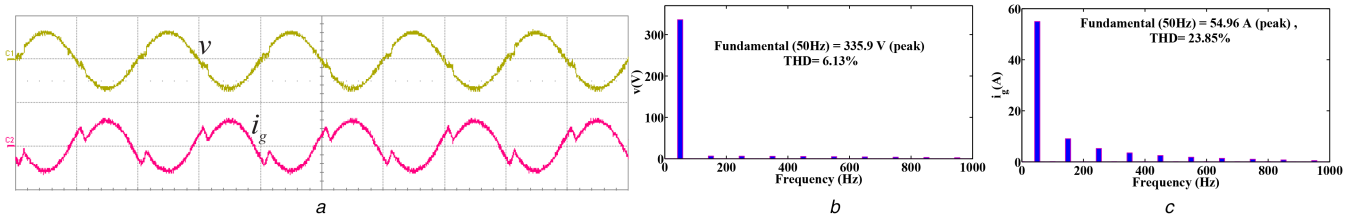

Fig. 6 *Harmonic performance with $P_{DG1} = P_{DG2} = 7.5$ kW*
(a) Waveforms of v and i_g, ***(b)*** Harmonic spectrum and THD of v, ***(c)*** Harmonic spectrum and THD of i_g

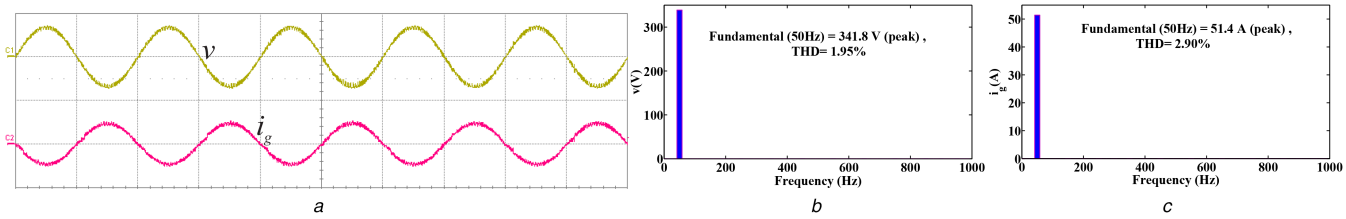

Fig. 7 *Harmonic performance with $P_{DG1} = P_{DG2} = 7.3$ kW*
(a) Waveforms of v and i_g, ***(b)*** Harmonic spectrum and THD of v, ***(c)*** Harmonic spectrum and THD of i_g

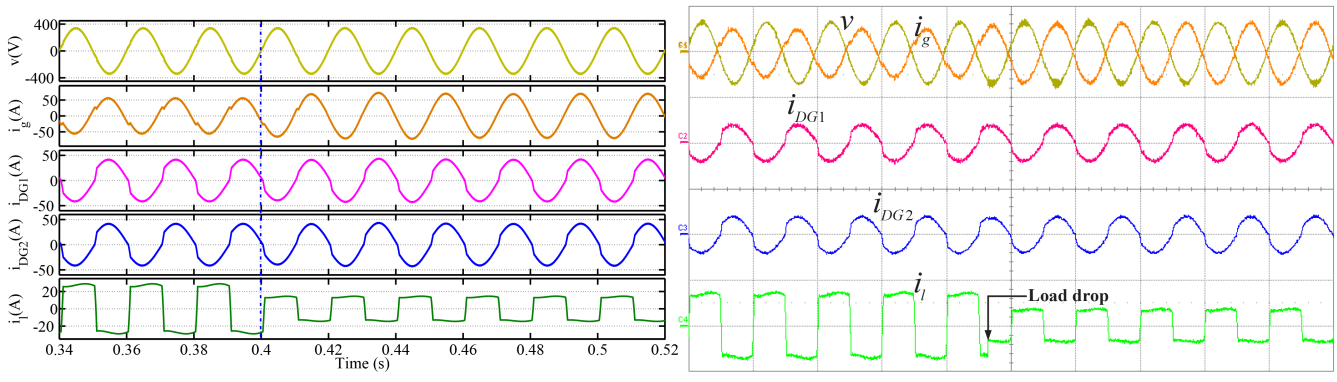

Fig. 8 *Performance under local load reduction with $P_{DG1} = P_{DG2} = 7.4$ kW*
(a) Simulation results, ***(b)*** Experimental results

4.2 Performance under load step change

The performances of the DG1 and the DG2 inverters under local loads change are shown in Figs. 8 and 9, respectively. The active power generation by the inverters in both DG systems is kept at 7.4 kW. Since the control algorithm utilises only the remaining capacities of the inverters to compensate the i_{lh} and i_{l1q} components of i_l, with $P_{DG1} = P_{DG2} = 7.4$ kW, the current i_{lh} alone is not being fully compensated. Therefore, the current i_g is still seen to be having harmonic distortion. Once the load connected to the system is reduced, the current i_g becomes sinusoidal as shown in Fig. 8. As the load decreases, the RMS values of i_{lh} and i_{l1q} decrease. Consequently, the inverters are able to compensate the currents i_{lh} and i_{l1q} present in i_l with their remaining capacities. Similarly, one can easily understand the performance when the load is applied back which is depicted in Fig. 9.

4.3 LVRT performance

The LVRT performance of the parallel-operated DG systems is shown in Fig. 10. During the fault, the PCC voltage is reduced by 0.5 pu and they system behaviour is depicted in Figs. 10*a* and *b*. Prior to the voltage drop, the inverters of DG1 and DG2 are feeding an active power of 7.3 kW. Since the remaining capacities

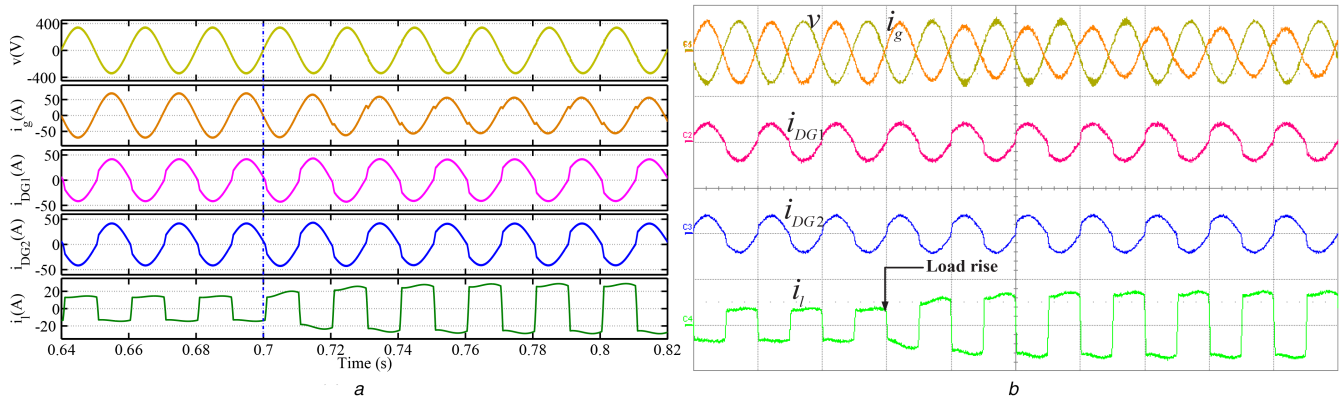

Fig. 9 *Performance under local load rise with* $P_{DG1} = P_{DG2} = 7.4\,kW$
(a) Simulation results, ***(b)*** Experimental results

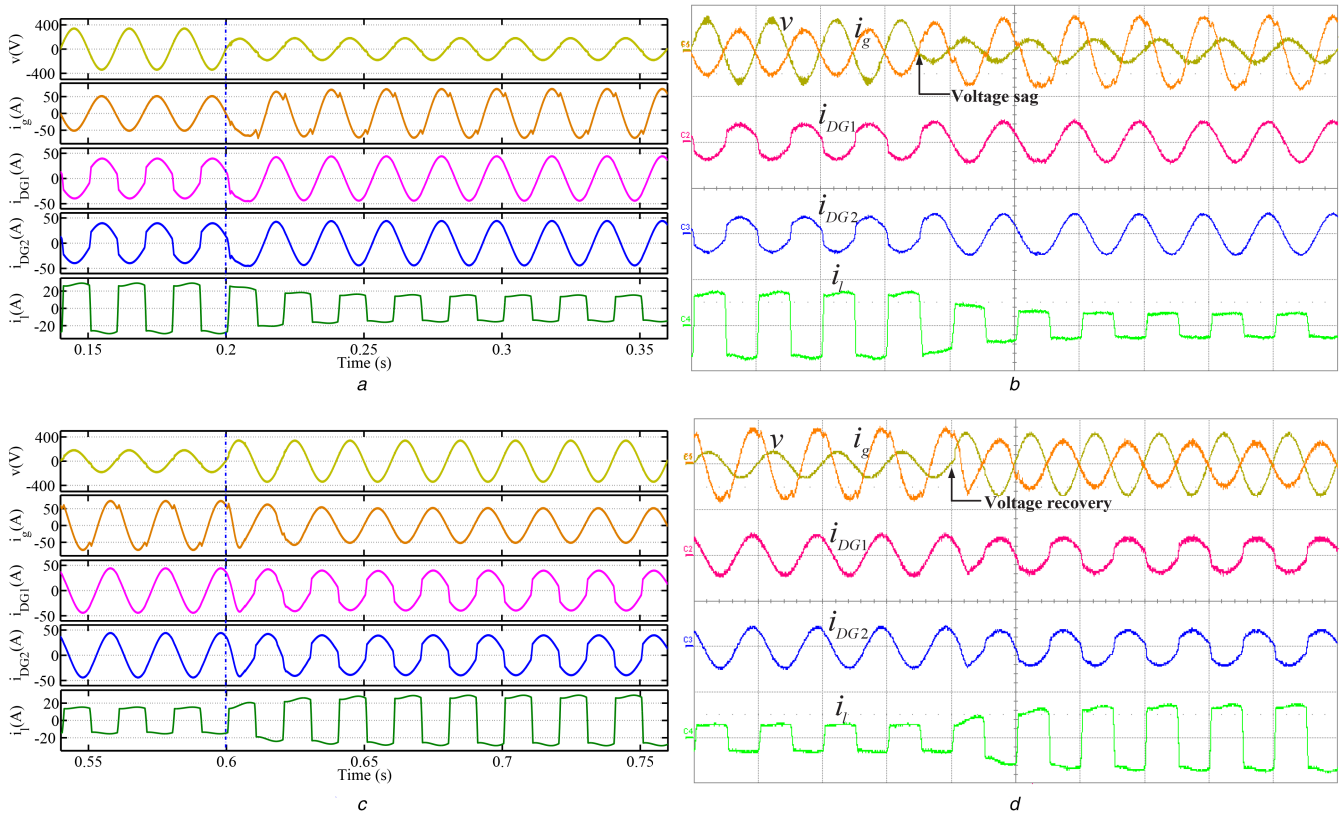

Fig. 10 *LVRT performance with* $P_{DG1} = P_{DG2} = 7.3\,kW$
(a), ***(b)*** During the grid voltage fall, ***(c)***, ***(d)*** During grid recovery

of the inverters are equal, they equally contribute to the compensations of i_{lh} and i_{l1q}. Moreover, it can be seen that they are able to fully compensate both i_{lh} and i_{l1q} with the available capacity before the fault. On sensing the reduction in PCC voltage, the LVRT feature of the control algorithm is activated, and then the operation of inverters in both DG systems is seamlessly transferred to LVRT mode. In LVRT mode, priority is given to reactive current injection. Once the inverter capacity is allocated for reactive current, then the remaining capacity is used for real current. During low voltage, the inverters start injecting reactive current as dictated by the grid codes and simultaneously decrease the real current component in order to accommodate the reactive current. Furthermore, during LVRT operation, the control algorithm sets the reference compensating currents i^*_{com1} and i^*_{com2} to zero and do not offer compensation of non-linear loads. Hence, harmonic distortion can be seen in the grid current i_g during the grid fault. The performance during the grid recovery from the fault is illustrated in Figs. 10*c* and *d*. As the grid voltage comes back to its normal condition, the operation of the inverters shifts back to the normal mode where the active power generation is given first priority and the compensation offered by the inverters is based on their excess capacities. Furthermore, it is noteworthy that the currents injected by the inverters of the DG system are well contained to their rated values during grid faults.

5 Conclusions

This paper has aimed at proposing and developing a coordinated control algorithm for parallel-operated MFDG systems fed from different renewable sources. The proposed control algorithm allocates only the excess capacity of the inverters for compensation purposes. The harmonic and reactive currents are distributed between the two inverters proportional to their remaining capacities. To extract the harmonic and reactive currents drawn by the local loads and estimate their RMS values, LMMN-based adaptive filtering has been used. Using the LMMN algorithm outputs, the proposed harmonic and reactive currents sharing algorithm has been developed. Besides harmonic and reactive currents compensation, the LVRT capability of the proposed control algorithm has also been covered. The simulation and experimental results presented in this paper demonstrate the

feasibility and effectiveness of the proposed control algorithm, which can be easily extended to any number of DG systems.

6 References

[1] Adefarati, T., Bansal, R.C.: 'Integration of renewable distributed generators into the distribution system: a review', *IET Renew. Power Gener.*, 2016, **10**, (7), pp. 873–884

[2] Trujillo, C., Santamaría, F., Gaona, E.: 'Modeling and testing of two-stage grid-connected photovoltaic micro-inverters', *Renew. Energy*, 2016, **99**, pp. 533–542

[3] Hajizadeh, A., Golkar, M.A.: 'Fuzzy neural control of a hybrid fuel cell/battery distributed power generation system', *IET Renew. Power Gener.*, 2009, **3**, (4), pp. 402–414

[4] Paiva, J., Carvalho, A.: 'Controllable hybrid power system based on renewable energy sources for modern electrical grids', *Renew. Energy*, 2013, **53**, pp. 271–279

[5] Blaabjerg, F., Chen, Z., Kjaer, S.B.: 'Power electronics as efficient interface in dispersed power generation systems', *IEEE Trans. Power Electron.*, 2004, **19**, (5), pp. 1184–1194

[6] Arzani, A., Venayagamoorthy, G.K.: 'Computational approach to enhance performance of photovoltaic system inverters interfaced to utility grids', *IET Renew. Power Gener.*, 2018, **12**, pp. 112–124(12)

[7] Maza Ortega, J.M., Gomez Exposito, A., Barragan Villarejo, M., *et al.*: 'Voltage source converter-based topologies to further integrate renewable energy sources in distribution systems', *IET Renew. Power Gener.*, 2012, **6**, (6), pp. 435–445

[8] Nian, H., Zeng, R.: 'Improved control strategy for stand-alone distributed generation system under unbalanced and non-linear loads', *IET Renew. Power Gener.*, 2011, **5**, (5), pp. 323–331

[9] Basaran, K., Cetin, N.S., Borekci, S.: 'Energy management for on-grid and off-grid wind/PV and battery hybrid systems', *IET Renew. Power Gener.*, 2017, **11**, (5), pp. 642–649

[10] Renders, B., Degroote, L., Driesen, J., *et al.*: 'Profits of power quality improvement by residential distributed generation'. 42nd Int. Universities Power Engineering Conf. 2007 UPEC 2007, Brighton, 2007, pp. 377–381

[11] Todeschini, G., Emanuel, A.E.: 'Wind energy conversion systems as active filters: design and comparison of three control methods', *IET Renew. Power Gener.*, 2010, **4**, (4), pp. 341–353

[12] Wu, J.C., Wu, K.D., Jou, H.L., *et al.*: 'Seven-level active power conditioner for a renewable power generation system', *IET Renew. Power Gener.*, 2014, **8**, (7), pp. 807–816

[13] Minambres Marcos, V., Guerrero Martinez, M.A., Romero Cadaval, E., *et al.*: 'Grid-connected photovoltaic power plants for helping node voltage regulation', *IET Renew. Power Gener.*, 2015, **9**, (3), pp. 236–244

[14] Shah, N., Rajagopalan, C.: 'Experimental investigation of a multifunctional grid interactive photovoltaic system operating in partial shading conditions', *IET Renew. Power Gener.*, 2016, **10**, (9), pp. 1382–1392

[15] Latran, M.B., Teke, A.: 'Investigation of multilevel multifunctional grid connected inverter topologies and control strategies used in photovoltaic systems', *Renew. Sustain. Energy Rev.*, 2015, **42**, pp. 361–376

[16] Boukezata, B., Gaubert, J.P., Chaoui, A., *et al.*: 'Predictive current control in multifunctional grid connected inverter interfaced by PV system', *Sol. Energy*, 2016, **139**, pp. 130–141

[17] Bouzelata, Y., Kurt, E., Altın, N., *et al.*: 'Design and simulation of a solar supplied multifunctional active power filter and a comparative study on the current detection algorithms', *Renew. Sustain. Energy Rev.*, 2015, **43**, pp. 1114–1126

[18] Ouchen, S., Betka, A., Abdeddaim, S., *et al.*: 'Fuzzy-predictive direct power control implementation of a grid connected photovoltaic system, associated with an active power filter', *Energy Convers. Manage.*, 2016, **122**, pp. 515–525

[19] Qazi, S.H., Mustafa, M.W.: 'Review on active filters and its performance with grid connected fixed and variable speed wind turbine generator', *Renew. Sustain. Energy Rev.*, 2016, **57**, pp. 420–438

[20] Naidu, N.K.S., Singh, B.: 'Experimental implementation of a doubly fed induction generator used for voltage regulation at a remote location', *IEEE Trans. Ind. Appl.*, 2016, **52**, (6), pp. 5065–5072

[21] Boutoubat, M., Mokrani, L., Machmoum, M.: 'Control of a wind energy conversion system equipped by a DFIG for active power generation and power quality improvement', *Renew. Energy*, 2013, **50**, pp. 378–386

[22] Chilipi, R.R., Al Sayari, N., Beig, A.R., *et al.*: 'A multitasking control algorithm for grid-connected inverters in distributed generation applications using adaptive noise cancellation filters', *IEEE Trans. Energy Convers.*, 2016, **31**, (2), pp. 714–727

[23] Bojoi, R.I., Limongi, L.R., Roiu, D., *et al.*: 'Enhanced power quality control strategy for single-phase inverters in distributed generation systems', *IEEE Trans. Power Electron.*, 2011, **26**, (3), pp. 798–806

[24] Al.Sayari, N., Chilipi, R., Barara, M.: 'An adaptive control algorithm for grid interfacing inverters in renewable energy based distributed generation systems', *Energy Convers. Manage.*, 2016, **111**, pp. 443–452

[25] Garanayak, P., Panda, G.: 'Fast and accurate measurement of harmonic parameters employing hybrid adaptive linear neural network and filtered-*x* least mean square algorithm', *IET Gener. Transm. Distrib.*, 2016, **10**, (2), pp. 421–436

[26] E.ON Netz GmbH: 'Grid code: high and extra high voltage' (E.ON Netz GmbH, Bayreuth, Germany, 2006)

[27] Moursi, M.S.E., Xiao, W., Kirtley, J.L.: 'Fault ride through capability for grid interfacing large scale PV power plants', *IET Gener. Transm. Distrib.*, 2013, **7**, (9), pp. 1027–1036

[28] Lin, F.J., Lu, K.C., Ke, T.H.: 'Probabilistic wavelet fuzzy neural network based reactive power control for grid-connected three-phase PV system during grid faults', *Renew. Energy*, 2016, **92**, pp. 437–449

[29] Saad, N.H., Sattar, A.A., Mansour, A.E.A.M.: 'Low voltage ride through of doubly-fed induction generator connected to the grid using sliding mode control strategy', *Renew. Energy*, 2015, **80**, pp. 583–594

[30] Alsayari, N., Chilipi, R., Al Hosani, K., *et al.*: 'Grid synchronization and control of distributed generation unit with flexible load compensation capabilities using multi-output LMS-filter', *International Journal Electric Power and Energy Systems*, 2017, **93**, pp. 253–265

[31] Hashempour, M.M., Savaghebi, M., Vasquez, J.C., *et al.*: 'A control architecture to coordinate distributed generators and active power filters coexisting in a microgrid', *IEEE Trans. Smart Grid*, 2016, **7**, (5), pp. 2325–2336

[32] Zeng, Z., Zhao, R., Yang, H.: 'Coordinated control of multi-functional grid-tied inverters using conductance and susceptance limitation', *IET Power Electron.*, 2014, **7**, (7), pp. 1821–1831

[33] Paredes, H.K.M., Bonaldo, J.P., Pomilio, J.A.: 'Centralized control center implementation for synergistic operation of distributed multifunctional single-phase grid-tie inverters in a microgrid', *IEEE Trans. Ind. Electron.*, 2018, **65**, (10), pp. 8018–8029

[34] Merai, M., Naouar, M., Slama Belkhodja, I.: 'Coordinated control of multiple multi-function grid connected converters for power quality improvement in microgrid applications'. 2016 Seventh Int. Renewable Energy Congress (IREC), Hammamet, 2016, pp. 1–6

[35] Cheng, P.T., Lee, T.L.: 'Distributed active filter systems (DAFSS): a new approach to power system harmonics', *IEEE Trans. Ind. Appl.*, 2006, **42**, (5), pp. 1301–1309

[36] Chambers, J., Tanrikulu, O., Constantinides, A.: 'Least mean mixed-norm adaptive filtering', *Electron. Lett.*, 1994, **30**, (19), pp. 1574–1575